This article was downloaded by:
On: *14 January 2011*
Access details: *Access Details: Free Access*
Publisher *Taylor & Francis*
Informa Ltd Registered in England and Wales Registered Number: 1072954 Registered office: Mortimer House, 37-41 Mortimer Street, London W1T 3JH, UK

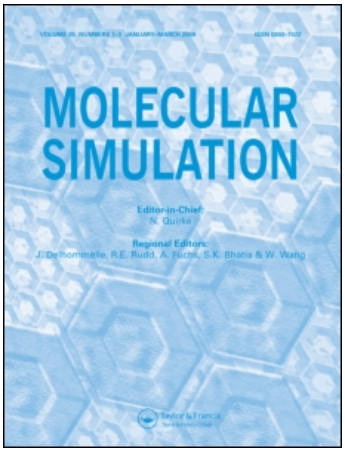

Molecular Simulation
Publication details, including instructions for authors and subscription information:
http://www.informaworld.com/smpp/title~content=t713644482

Structure of saccharose-based carbon and transport of confined fluids: hybrid reverse Monte Carlo reconstruction and simulation studies

T. X. Nguyen[a]; S. K. Bhatia[a]; S. K. Jain[b]; K. E. Gubbins[b]
[a] Division of Chemical Engineering, The University of Queensland, Brisbane, Australia [b] Department of Chemical and Biomolecular Engineering, North Carolina State University, Raleigh, NC, USA

To cite this Article Nguyen, T. X. , Bhatia, S. K. , Jain, S. K. and Gubbins, K. E.(2006) 'Structure of saccharose-based carbon and transport of confined fluids: hybrid reverse Monte Carlo reconstruction and simulation studies', Molecular Simulation, 32: 7, 567 — 577
To link to this Article: DOI: 10.1080/08927020600675699
URL: http://dx.doi.org/10.1080/08927020600675699

PLEASE SCROLL DOWN FOR ARTICLE

Full terms and conditions of use: http://www.informaworld.com/terms-and-conditions-of-access.pdf

This article may be used for research, teaching and private study purposes. Any substantial or systematic reproduction, re-distribution, re-selling, loan or sub-licensing, systematic supply or distribution in any form to anyone is expressly forbidden.

The publisher does not give any warranty express or implied or make any representation that the contents will be complete or accurate or up to date. The accuracy of any instructions, formulae and drug doses should be independently verified with primary sources. The publisher shall not be liable for any loss, actions, claims, proceedings, demand or costs or damages whatsoever or howsoever caused arising directly or indirectly in connection with or arising out of the use of this material.

Molecular Simulation, Vol. 32, No. 7, 15 June 2006, 567–577

Taylor & Francis
Taylor & Francis Group

Structure of saccharose-based carbon and transport of confined fluids: hybrid reverse Monte Carlo reconstruction and simulation studies

T. X. NGUYEN†, S. K. BHATIA†*, S. K. JAIN‡ and K. E. GUBBINS‡

†Division of Chemical Engineering, The University of Queensland, Brisbane, QLD 4072, Australia
‡Department of Chemical and Biomolecular Engineering, North Carolina State University, 911 Partner's Way, Raleigh, NC 27695-7905, USA

(Received December 2005; in final form March 2006)

We present results of the reconstruction of a saccharose-based activated carbon (CS1000a) using hybrid reverse Monte Carlo (HRMC) simulation, recently proposed by Opletal *et al.* [1]. Interaction between carbon atoms in the simulation is modeled by an environment dependent interaction potential (EDIP) [2,3]. The reconstructed structure shows predominance of sp^2 over sp^3 bonding, while a significant proportion of sp hybrid bonding is also observed. We also calculated a ring distribution and geometrical pore size distribution of the model developed. The latter is compared with that obtained from argon adsorption at 87 K using our recently proposed characterization procedure [4], the finite wall thickness (FWT) model. Further, we determine self-diffusivities of argon and nitrogen in the constructed carbon as functions of loading. It is found that while there is a maximum in the diffusivity with respect to loading, as previously observed by Pikunic *et al.* [5], diffusivities in the present work are 10 times larger than those obtained in the prior work, consistent with the larger pore size as well as higher porosity of the activated saccharose carbon studied here.

Keywords: Reverse Monte Carlo; Carbon; Pore size distribution; Diffusivity

Downloaded At: 18:02 14 January 2011

1. Introduction

Porous carbons have long been used for gaseous and liquid phase adsorptive separations as well as storage of volatile compounds, because of their high surface area and the strong adsorption forces arising from a high site density of close packed sp^2 carbon atoms in graphitic structure. The synthesis and manufacture of carbons with desired adsorptive properties requires reliable characterization of the internal structure of the carbon, which can be used for predicting adsorption equilibrium and kinetics from a mature understanding of the behavior of fluids in confined spaces. However, in practice the microstructure of porous carbon is complex and poorly understood due to its highly disordered nature. This leads to difficulty in accurately characterizing the pore morphology and topology even with modern visualization techniques such as high-resolution transmission electron microscopy (HRTEM), or by X-ray diffraction (XRD) and small angle X-ray scattering. Consequently, the traditional indirect method of characterization in terms of an idealized structural model, based on analysis of gas adsorption data, is still the most commonly employed technique, and provides a powerful complement to the above methods for interpreting the internal structure of porous carbons.

The slit–pore model, in which the microstructure of porous carbon is modeled as an ensemble of independent graphitic pores, has been widely utilized for the characterization of the microstructure of porous carbons [6–8] based on gas physisorption. Recently, the traditional slit–pore model, considering infinitely thick walls, has been extended to consider finite walls with a distribution of wall thickness in our laboratory [6,9–11]. Although the characterization is significantly improved by our approach, the finite wall thickness (FWT) model, the slit–pore model in general disregards roughness of the carbon surface and pore connectivity effects, which may have significant impact on dynamic properties of adsorption [12]. Consequently, it is useful to investigate alternate more realistic models that can facilitate validation and testing of the slit–pore model.

Atomistic reconstruction of the microstructure of nanoporous carbons offers a promising alternative for

*Corresponding author. Email: sureshb@cheque.uq.edu.au

Molecular Simulation
ISSN 0892-7022 print/ISSN 1029-0435 online © 2006 Taylor & Francis
http://www.tandf.co.uk/journals
DOI: 10.1080/08927020600675699

developing realistic models of the carbon structure, avoiding *ad hoc* assumptions of the slit–pore model. In this direction, early attempts to reconstruct highly activated carbons used a reverse Monte Carlo (RMC) method [13] involving fitting of experimental pair correlation functions obtained using scattering methods. Subsequent work by Gubbins *et al.* [14–16] has considered also geometric constraints on bond length, bond angle and sp^2/sp^3 bonding ratio. Pikunic *et al.* [15,16] showed that simulated transmission electron microscopy (TEM) images of the reconstructed carbons agree qualitatively with corresponding TEM images, measured on the real carbons. Further, these authors also showed that the reconstructed carbon models are able to quantitatively predict the isosteric adsorption of argon at 77 K [17]. Although the RMC method using the geometric constraints is computationally attractive while providing a preliminary atomistic carbon model, it may not guarantee stable structures as it predicts a significant fraction of three-member rings [18]. While the fit may be improved by adjusting the weighting factors for the bond angle and neighbor constraints, relative to $g(r)$, this leads to unreasonably high levels of three- and four-member rings. Furthermore, the RMC method with the graphite constraints does not seem to provide a good fit between the simulated pair correlation function and the target one for highly disordered carbons [19].

A recently proposed hybrid reverse Monte Carlo (HRMC) method [1], combining the conventional RMC method with an energy-based constraint, has been shown to improve stability of the structure, as it yields a much smaller fraction of three-member rings compared with that obtained using the conventional RMC method. The HRMC method equipped with the Marks potential [2,3] has been recently applied to reconstruction of several high-density non-porous carbons [20–22]. In a more recent work [23], the HRMC method has been applied by Jain *et al.* to saccharose-based porous carbons, using the reactive empirical bond order potential (REBO) of Brenner [24] to model the interactions between the carbon atoms. The hydrogen atoms are also treated explicitly in their simulation method and the carbon–hydrogen and hydrogen–hydrogen interactions are modeled using the REBO potential.

In this paper, we employed the HRMC method to reconstruct a saccharose-based activated carbon, named CS1000a, studied recently by Jain *et al.* [19,23]. This carbon was obtained by activation of a non-porous carbon, CS1000, in a CO_2 atmosphere for 20 h [19]. Argon is used as a spherical molecule probe, as previously used by Thomson and Gubbins [14], to determine a pore size distribution (PSD). The geometrical PSD is then used to validate that obtained from interpretation of the argon adsorption isotherm at 87 K, using our recently proposed model, the FWT model and the traditional IWT model. For this, simulated experimental data of the argon adsorption isotherm at 87 K is generated using Grand Canonical Monte Carlo (GCMC) simulation. Further, we also determine the self-diffusivity of argon at 87 K and nitrogen at 77 K in the reconstructed carbon using equilibrium molecular dynamics (EMD) simulation.

2. Simulation details

In the present work, we utilized the HRMC technique [1,23], which combines the conventional RMC [13] method with an energy constraint. The HRMC method involves sampling configurations in the canonical ensemble in which the number of particles, N, volume of the simulated system, V and temperature, T, are held constant, such that a minimum in deviation for a suitable target objective function and in total energy of the simulated system is simultaneously achieved. The most commonly used target objective functions are the experimental structure factor, $S(Q)$ and the pair correlation, $g(r)$. The trial configuration is generated by random movement of a carbon atom in the simulated system with the acceptance probability, P, given as:

$$P = \mathrm{e}^{-\chi^2/2}\mathrm{e}^{-\Delta E/kT} \tag{1}$$

The first term in the right hand side is the acceptance probability used in the conventional RMC method. In this work, we employed the pair correlation function as the objective function. Accordingly, the quantity, χ, is defined by:

$$\chi^2 = \sum_{i=1}^{N_{\mathrm{exp}}} \frac{((g(r_i))_{\mathrm{RMC}} - (g(r_i))_{\mathrm{EXP}})^2}{\sigma(r_i)^2} \tag{2}$$

where $(g(r_i))_{\mathrm{RMC}}$ is the simulated pair correlation function, calculated from the simulated configuration and $(g(r_i))_{\mathrm{EXP}}$ is the target pair correlation function, taken from Jain *et al.* [19,23], and was determined from the experimental structure factor, $S(Q)$, using the Monte Carlo $g(r)$ (MCGR) method [25], described in detail elsewhere [15]. $\sigma(r_i)$ is the experimental error. In this work, $\sigma(r_i)$ is kept constant for all the experimental data points, N_{exp}, and utilized as an adjustable parameter.

The second term in the right hand side is the acceptance probability used in conventional Metropolis Monte Carlo (MMC) simulation or energy based constraint, that penalizes formation of highly strained rings such as three- and four-member rings. Here, ΔE is the difference in total energy of the system between new and old configurations. The new configuration is generated when a carbon atom in the system is moved. The total energy of the simulated system is determined using the environment dependent interaction potential (EDIP), recently developed by Marks [2,3] for carbon. In particular, the total energy, E, is given as a sum of the energy of individual atoms in the simulated system, U_i,

$$U_i = \sum_j U_2(r_{ij}, Z_i) + \sum_{j<k} U_3(r_{ij}, r_{ik}, \theta_{jik}, Z_i) \tag{3}$$

Downloaded At: 18:02 14 January 2011

Downloaded At: 18:02 14 January 2011

where the terms U_2 and U_3 are pair and three body interaction potentials, respectively. The potentials are dependent upon not only interatomic distance and bond angle but also the generalized coordination number, Z_i. The latter is determined from a spherical coordination component, z_i, defined as the sum of distance-based weight functions of all the first nearest neighbors of the centered atom, i and non spherical terms, X_i, representing local geometrical constraints consisting of dihedral rotation and repulsions between π orbitals at twofold and threefold sites. The complete expression of Z_i is given as:

$$Z_i = z_i + \pi_3(z_i)X_i^{\text{dih}} + \pi_3(z_i)X_i^{\text{rep3}} + \pi_2(z_i)X_i^{\text{rep2}} \quad (4)$$

where π_2 and π_3 are switching functions to identify two- and three-coordinated atoms.

In the current work, we employed a simulated annealing algorithm, proposed by Kilpatrick [26] and introduced in [16], to reconstruct the carbon. Accordingly, multiple canonical ensembles are employed in the reconstruction procedure. The number of carbon atoms, N and simulation volume, V, are kept constant for all the ensembles while the temperature, T_{anneal}, for an individual ensemble varies as follows:

$$T_{\text{anneal}} = T_0 a^{N_{\text{anneal}}} \quad (5)$$

Here, T_0 is the initial temperature of the annealing process. We choose the carbon liquid state as the initial carbon structure, or $T_0 = 5000$ K. The parameter, a, is not greater than unity and considered as an annealing rate. We used $a = 0.97$ in the present work. Finally, N_{anneal} is the number of annealing steps, determined from the above equation if the final temperature of annealing process is assigned. We set the final temperature, $T_F = 300$ K. This temperature approximates that at which the experimental structure factor is measured. Further, the adjustable parameter, σ, varies in accordance with following equation:

$$\sigma_{\text{anneal}} = \sigma_0 a^{N_{\text{anneal}}/2} \quad (6)$$

where the initial value, σ_0, is determined such that σ_{anneal} at the convergence state or $\sigma_{\min}$ approximates the experimental error in the radial correlation function, $g(r)$. The adjustable parameter, σ_0, is generally sufficiently large to allow the system to pass over local minima of the space (χ, E).

In this work, we applied the HRMC technique, described above, to reconstruct saccharose-based carbon (CS1000a). The preparation procedure of the carbon has been detailed by Jain *et al.* [19]. The carbon density, ρ_C and experimental pair correlation function $(g(r))_{\text{EXP}}$ of this carbon is also taken from Jain *et al.* [19]. The former ($\rho_C = 0.7218$ g/cm^3) is calculated from the chemical compositions and bulk density of the carbon, determined using mercury pycnometry. The use of this density in HRMC simulation entails the assumption that the carbon is predominantly microporous, as macropores are of too large a length scale to be accessed by this method. In order to investigate the impact of the adjustable parameter, $\sigma_{\min}$, on reconstructed structure of the carbon we first simulated a small system with 125 carbon atoms in a cubic simulation box whose size is 15.112 Å. Subsequently, we simulated a larger system with 566 carbon atoms in a cubic simulation box whose size is 25 Å. Detailed discussion of the results of the reconstruction is provided in a later section.

3. Reconstruction of the saccharose-based activated carbon (CS1000a)

3.1 Small system

We performed several HRMC simulations with increasing value of the adjustable parameter, $\sigma_{\min}$, ranging from 0.045 to 0.067. Five million Monte Carlo (MC) steps are used in all the simulations. Figures 1a, b and 2 show in turn variations in the quantity, χ^2 and total energy of simulated systems with respect to number of Monte Carlo steps. From figure 1a, it can be seen that the values of the quantity χ^2 for three HRMC simulations converge to very similar values after 5 million MC steps. Figure 1b also shows that the simulated pair correlation function of the

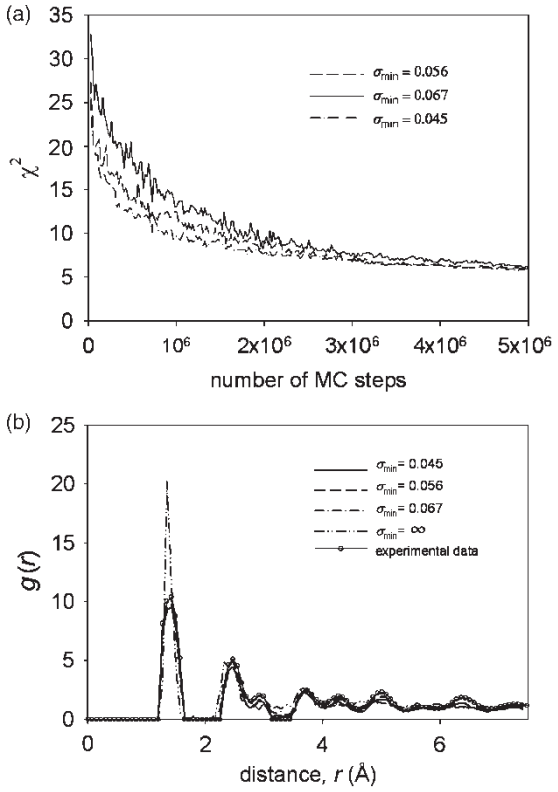

Figure 1. (a) Effect of minimum weighting parameter, $\sigma_{\min}$, on the evolution of the fitting parameter, χ^2; (b) comparison of target and converged simulated pair correlation function, for different minimum values of weighting parameter, $\sigma_{\min}$. The symbol ∞ represents Metropolis Monte Carlo simulation.

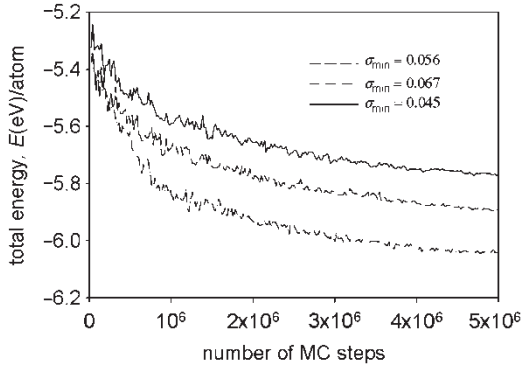

Figure 2. Effect of minimum weighting parameter, σ_{min}, on evolution of total energy (E) of the simulated system. Total energy E is divided by the number of carbon atoms in the simulated system.

final configuration of these three simulations matches reasonably well to the experimental one. However, as seen in figure 2, the total energy of the three corresponding configurations after 5 million MC steps is significantly different. In particular, the total energy decreases with increasing weighting parameter, σ_{min}. Such decrease in total energy is associated with significant reduction in the fraction of three-member rings, as seen in figure 3. This can also be directly observed in figures 4a–c. Thus, minimization of the difference between target and simulated pair correlation function, $g(r)$, corresponding to the conventional RMC method, does not lead to a physically realistic structure.

Based on the above observations, we performed several HRMC simulations with very high values of minimum weighting parameter, σ_{min} or energetically favorable weighting, to minimize the fraction of three-member rings. It was found that increasing the minimum weighting parameter, σ_{min}, leads to an increase in the quantity χ^2 at convergence, although a significant reduction in fraction of three-member rings and total energy of the final configuration is obtained. Figure 4d provides a snapshot of the configuration after 5 million MC steps using MMC simulation. From this figure and figure 3a, it can be seen

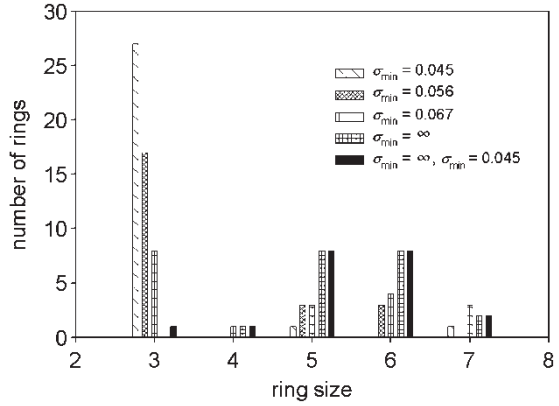

Figure 3. Effect of minimum weighting parameter, σ_{min}, on distribution of ring size of the simulated systems. The symbol ∞ depicts MMC simulation.

that there is still one three-member ring even though only energetic constraint was applied. This three-membered ring persists as more configurations are sampled and the energy remains unchanged. This is normally observed in even final configuration of high-density carbon from *ab initio* MD calculation [27]. Further, the total energy of the final MMC configuration is at its lowest value ($E = -6.32$ eV/atom) in comparison with that of the HRMC simulations. From figure 1b, the simulated pair correlation function calculated from the final MMC configuration significantly deviates from the corresponding experimental one, especially for the first peak that represents short-range order. This is due to the fact that the EDIP potential treats all bond types in carbon as conjugated bonds [2]. Consequently, the distance corresponding to conjugated bond length is energetically favorable. This leads to the sharpness of the first peak in the simulated pair correlation function in comparison with that of the experimental pair distribution function.

Interestingly, if we employ the final MMC configuration as the initial configuration for the HRMC simulation at 300 K and select an appropriate value of the weighting parameter, σ, we obtained a reasonable structure after 5 million MC steps. In particular, figure 5 shows that the simulated pair correlation function matches reasonably well with the corresponding experimental one. Further, the ring statistics distribution, determined using the shortest path criterion of Franzblau [28] and total energy of the simulated structure are very similar to those calculated from the MMC configuration although fitting to the experimental pair distribution function is slightly worse in the long range region (>6 Å). The latter may be due to inaccuracy of the interaction potential model in this region, arising from the cut-off employed. Thus, implementation of HRMC simulation at low temperature such as 300 K provides an advantage in improving the fit between the simulated and experimental pair correlation functions while not creating any more three-member rings.

3.2 Large system

We next applied the results obtained for the small system to a larger system that consists of 566 carbon atoms in a cubic box whose sides have length of 25 Å. In particular, the procedure comprises two main steps.

3.2.1 Preparation of initial configuration. In this initial step, HRMC simulation in conjunction with the annealing scheme is conducted, as described in section 2. Appropriate selection of a high value of the minimum weighting parameter, σ_{min}, must be made such that the final configuration contains a minimum fraction of three-member rings. To reduce computation time, we employed the REBO potential [24] in the HRMC simulation in this

Downloaded At: 18:02 14 January 2011

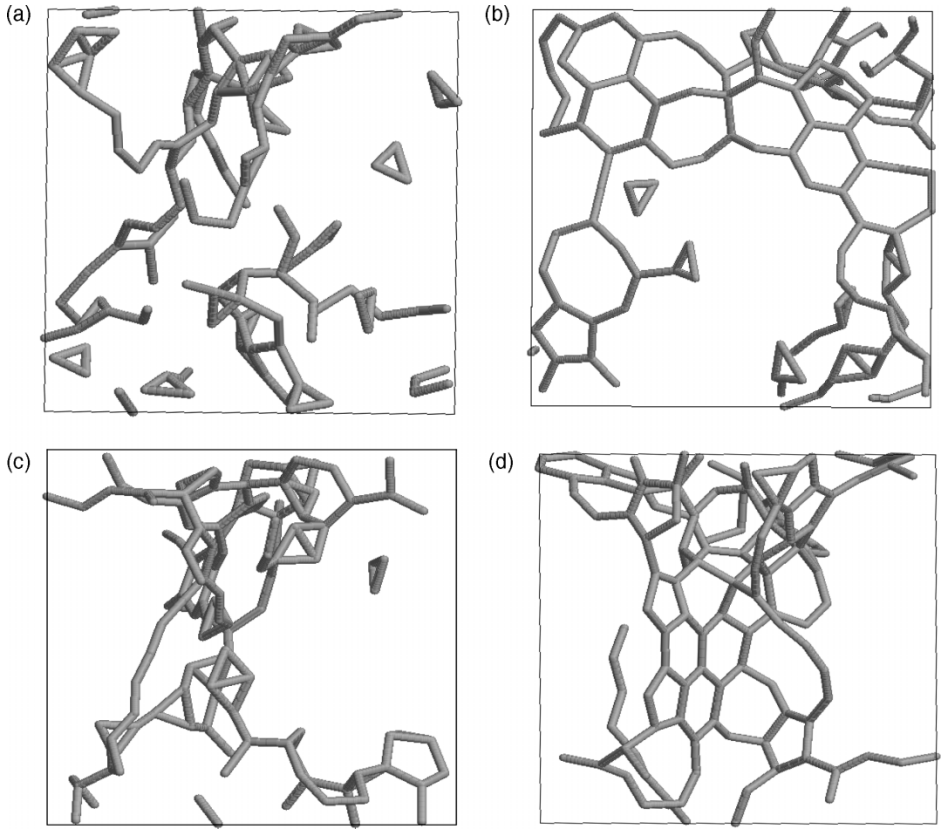

Figure 4. Snapshots of final configuration of simulated systems for different minimum values of weighting parameter, σ_{min}: (a) $\sigma_{min} = 0.045$; (b) $\sigma_{min} = 0.056$; (c) $\sigma_{min} = 0.067$; (d) $\sigma_{min} = \infty$ for first step using MMC simulation and $\sigma_{min} = 0.045$ for the second step using HRMC simulation at 300 K.

Downloaded At: 18:02 14 January 2011

step with acceptance criteria given by Jain *et al.* [23]

$$P = \min\left[1, \exp\left(-\frac{1}{T_\chi}\left(\left(\chi^2_{new} - \chi^2_{old}\right) + \frac{\Delta E}{w}\right)\right)\right] \quad (7)$$

where T_χ a fictitious temperature and w is weighting parameter used for the energy term. χ^2 is defined as:

$$\chi^2 = \sum_{i=1}^{N_{exp}} \left[(g(r_i))_{RMC} - (g(r_i))_{EXP}\right]^2 \quad (8)$$

Thus, the acceptance criteria given in equation (7) is same as that given in equation (1) if T_0 and σ_0 are expressed as:

$$\sigma_0 = \sqrt{\frac{T_\chi}{2}} \quad (9)$$

$$T_0 = \frac{wT_\chi}{k} \quad (10)$$

The appropriate choice of weighting factors w and T_χ or (T, T_0, σ_0, σ_{min}) is taken. This short-ranged potential does not take into account non π-bonding interactions. The latter requires a time-consuming computation. In particular, the total energy is given as the sum of the energy of a pair of covalently bonded atoms, E_{ij}. The latter is expressed as:

$$E_{ij} = V^R_{ij}(r_{ij}) + b_{ij}V^A_{ij}(r_{ij})$$

where V^R_{ij} and V^A_{ij} are repulsive and attractive pairwise potentials, respectively. The potentials are only dependent upon interatomic distance. The attractive potential is weighted by the bond order term, b_{ij}, that represents various chemical effects, contributed by atoms close to the i–j bond, on the strength of the covalent bond between atom i and j. Thus, the REBO potential considers only bonded interactions, while the EDIP potential considers not only bonded but also non-bonded interactions. The short-ranged nature of the REBO potential is represented

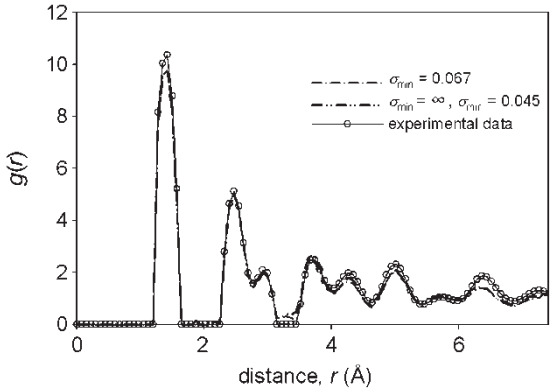

Figure 5. Comparison of simulated pair correlation functions of two final configurations with experimental data. HRMC technique was used for the first simulated system while MMC and then HRMC simulations were used for the second simulated system.

by the bond order term, b_{ij}, whose cut-off is 2 Å. The longer-ranged nature of the EDIP potential can be seen through consideration of non-bonded interaction of π orbitals between two carbon sheets. These interactions are given by the non-spherical terms, X_i, representing local geometrical constraints consisting of dihedral rotation and repulsions between the π orbitals at twofold and threefold sites. These terms, X_i, have the cut-off of 3.2 Å and require intensive computation. Consequently, the EDIP potential requires more computation than the REBO potential, and the latter is, therefore, used generate the initial configuration for HRMC simulation. However, the EDIP potential is preferably employed to obtain the final configuration in the current work instead of the adaptive intermolecular REBO (AIREBO) potential [29], an extended version of the REBO potential with consideration of non-bonded interactions. This is because of the greater accuracy of the former potential, which has been shown to provide structural properties of simulated carbon structure such as bond length, bond angle and coordination number distribution similar to those obtained from the highly accurate models [2,30]. On the other hand, the AIREBO potential gives structural properties that differ significantly from those using accurate *ab initio* and tight binding methods [31,32].

The above configuration is used as the initial configuration for the HRMC simulation at 300 K. Figure 6a depicts the pair correlation function (dash-dotted line) of this configuration compared with corresponding experimental data, showing that the first peak of the simulated pair correlation function is very sharp with much higher intensity compared with the corresponding experimental one. This observation is due to an energetically favored fit, as explained in section 3.1. The energetically favorable fit leads to minimized formation of three-member rings, as seen in figure 7a, with the structure having a predominance of sp^2 bonding type, as seen in figure 7b. From figure 8 it is evident that a bond angle of 120° in the structure is also predominant, while there is a small proportion of bond angle of 60° that indicates existence of a few three-member rings.

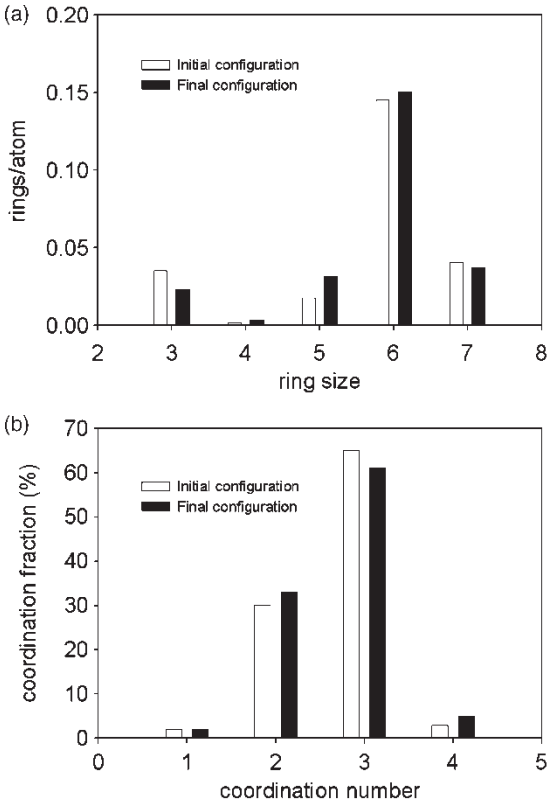

Figure 7. (a) Comparison of distribution of ring size between the initial and converged configurations of the large simulated system (566 carbon atoms); (b) comparison of distribution of coordination number for these two configurations.

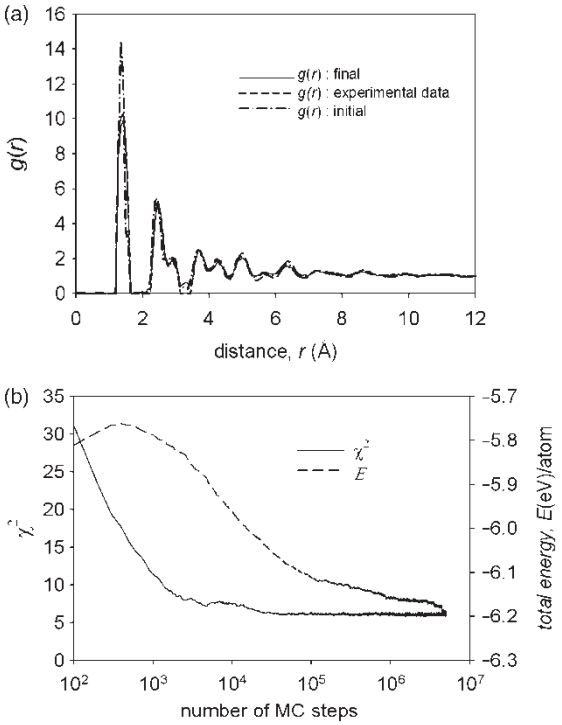

Figure 6. (a) Comparison of pair correlation function of the initial configuration and converged configuration of the large simulated system (566 carbon atoms) with the experimental one and (b) evolution of fitting parameter, χ^2 and total energy (E) of the large simulated system (566 carbon atoms). Total energy E is divided by total number of carbon atoms in the simulated system.

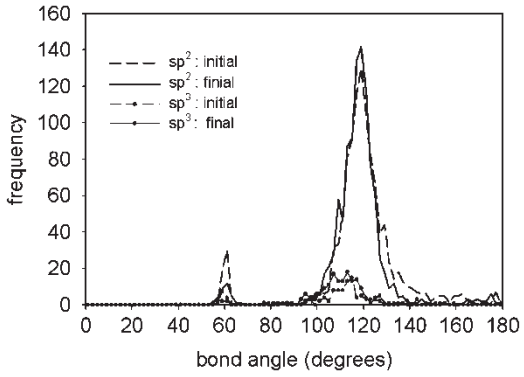

Figure 8. Comparison of distribution of bond angle for sp^2 and sp^3 bond types, between initial and converged configurations of the large simulated system (566 carbon atoms).

Downloaded At: 18:02 14 January 2011

3.2.2 Improvement of simulated structure. The final configuration from the first step is employed as the initial configuration in the HRMC simulation in this step. The HRMC simulation was performed at 300 K for the first step for 5 million MC steps. Figure 6b depicts the variation in the quantity, χ^2 and total energy of the system, E, during the simulation. From this figure, χ^2 and E decrease simultaneously after the first few 100 MC steps, and level off after 4 million MC steps. The latter indicates convergence of the system, whereby the simulated structure is invariant in terms of pair distribution function and total energy.

Figure 6a shows the pair correlation function of the converged configuration compared with the corresponding experimental one. From this figure, we can see an excellent fit between the two quantities even in the long range region, while the total energy is much lower than that of the initial configuration, and approaches that of the configuration obtained for the small system, as mentioned in the section 3.1. Such better fit in the long-range region may be due to the fact that the initial configuration used in this stage was prepared using HRMC simulation instead of MMC simulation. The former provides a good fit between simulated and experimental pair correlation functions in the long range, as in the region of around 6 Å in figure 6a. For this region a similar good fit was not achieved for the small system, as seen in figure 5. This better fit is achieved here by adjusting the weighting factor to better fit the pair correlation constraint, which compensates the inaccuracy of the EDIP potential at long range. Further, the converged structure contains a smaller number of three-membered rings compared to the input configuration, as well as additional formation of five and six member rings, as seen in figure 7a. This can also be seen from the significant reduction in frequency of bond angles of 60° and a slight increase in frequency of bond angles at 120°, as seen in figure 8. Figure 7b shows that there is additional formation of sp and sp^3 bond types associated with disappearance of a small number of sp^2 type bonds. Here two atoms are considered to be bonded if the distance between these two atoms is less than 1.85 Å. This bonding criterion was used by Marks [2,3] to calculate coordination number of nonporous carbon. Finally, it is noted that the structural characteristics used to analyze the initial and converged structures in the present work, such as ring distribution, coordination number and bond angle distribution are very similar while their pair correlation function and total energy are significantly different. Accordingly, these structural characteristics seem to be insufficient to represent the basic properties of carbon structure. In general, one expects such characteristics to reflect more the short-range features of the structure, so that the long-range part of $g(r)$ can be significantly different for structures having similar coordination number and bond length distribution.

Figure 9 illustrates a snapshot of a unit cell of the converged structure of the saccharose-based carbon (CS1000a). It can be observed that a significant number of carbons are connected to each other through sp and sp^3 type bonds, leading to formation of complex pore morphology. This illustrates the nature of very low-density carbon whose microstructure is highly disordered. This issue will be further discussed in a later section.

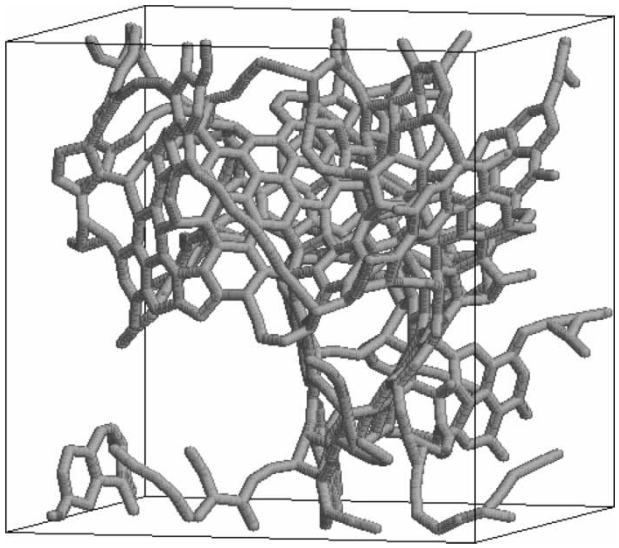

Figure 9. Snapshot of converged configuration of the large simulated system (566 carbon atoms).

4. Characterization of the reconstructed carbon

In this section, we perform characterization of the reconstructed carbon (CS1000a) using the spherical probe method [14], first introduced by Gelb and Gubbins [33] to find the exact geometric PSD, as well as with the FWT and IWT models. The spherical probe method is known to provide a geometric PSD that can compared with those obtained from the FWT and IWT models. Argon is modeled as a Lennard–Jones (LJ) particle and employed as the probing molecule. We utilized a value of the LJ collision diameter for argon, $\sigma_{Ar-Ar} = 3.395$ Å and cross-collision diameter between argon and carbon, used as cutoff radius in the method, $\sigma_{Ar-C} = 3.41$ Å. For estimation of the PSD using the FWT model, we determined the argon adsorption isotherm at 87 K using grand canonical MC simulation. This was then used as the simulated experimental adsorption isotherm in the carbon. A cut-off value, $r_c = 12.4$ Å, was used in the simulation. LJ parameters for fluid–fluid interaction and solid–fluid interaction were taken from Dombrowski *et al.* [34].

In figure 10a, empty circles depict argon adsorption isotherms at 87 K obtained using GCMC simulation, while the solid and dash lines represent fitted adsorption isotherms obtained from matching the simulated adsorption isotherm using the FWT and IWT models, respectively. It is seen that the FWT model does not provide good fit to the simulated adsorption isotherm in the region of relative pressure between 5×10^{-5} to 10^{-3} and 3×10^{-3} to 2×10^{-2}. Deviation of the fitted

Downloaded At: 18:02 14 January 2011

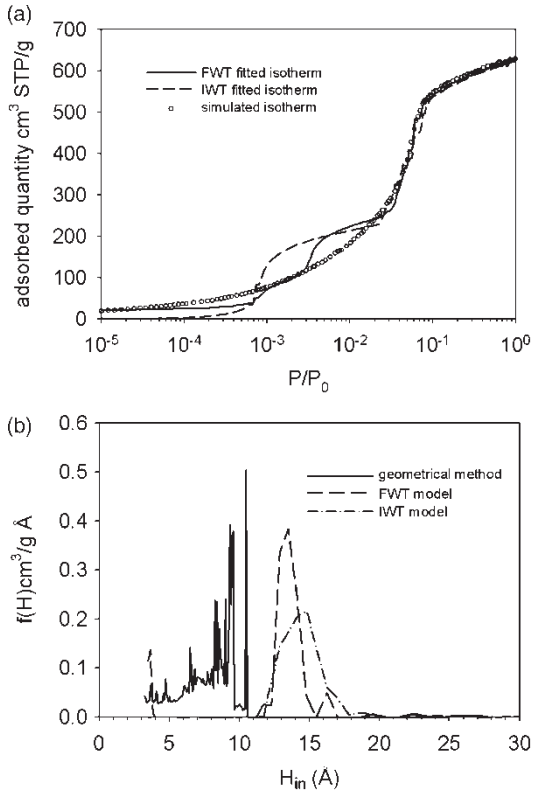

Figure 10. (a) Comparison of adsorption isotherm of argon at 87 K obtained using GCMC simulation (open circles) and the fitted isotherms from the fit of FWT and IWT models to the simulated adsorption data; (b) results of PSD obtained using spherical probe method and using the FWT and IWT models.

isotherm from the simulated one was also observed for high surface area activated carbon fibers, reported in our previous work [6]. However, such deviation for the case of the investigated activated carbon fibers is smaller by many orders of magnitude than that observed in the current work. The deviation is due to the disregard of surface heterogeneities arising from the presence of defects leading to roughness of surface as well as its curvature. Such heterogeneities are more significantly pronounced as the thickness of carbon walls decreases, as discussed in our previous work [6]. From the figure 9 it can be observed that carbon sheets are small, curved and distorted due to defects. Accordingly, the reconstructed structure of the investigated carbon is much less graphitized than those studied in our previous works [6,9]. This may be due to very low density of the carbon. On the other hand, the fitted adsorption isotherm obtained using the IWT model matches with the simulated one only at high relative pressure ($>3 \times 10^{-2}$). Similar results were reported for porous glasses by Figueroa-Gerstenmaier *et al.* [35]. Accordingly, the FWT model is superior to the IWT model for characterization of highly disordered carbon.

Figure 10b depicts the actual geometrical PSD (real PSD) and predicted PSD obtained from the fit of the simulated argon adsorption isotherm using the FWT and IWT models. It is noted that the PSD of activated carbons obtained using gas adsorption is commonly seen to distribute predominantly in the micropore range (<20 Å). Accordingly, the simulation box size (25 Å) used in the current work enables detection of the micropore range below this size, although an upper bound of the PSD of the investigated carbon (CS1000a) can only be determined by other techniques such as gas adsorption. Here, we note that Figueroa-Gerstenmaier *et al.* [35] showed that the geometrical PSD of simulated porous glasses using spherical probes agrees reasonably well with that obtained using IWT model with slit and cylindrical geometries. From this figure, it can be seen that the first peak of the predicted PSD (dashed line in the neighborhood of 4 Å pore size) obtained from the FWT model is located in the first region of the geometrical PSD while the second and major peak of the predicted PSD is shifted by about 3.4 Å from the major peak of the geometrical PSD. The former results from the good agreement of the fitted isotherm using the FWT model with the simulated one at low relative pressure, as seen in figure 10a. Furthermore, pores in the interval of 4–10 Å, observed for the geometrical PSD, are completely absent in the predicted PSD obtained using the FWT model. These deviations are due to the significant deviation of the FWT derived-isotherm from the simulated one, as explained in detail in the above paragraph. However, the intensity of the second peak of the predicted PSD using the FWT model agrees reasonably well with that of the major peak of the geometrical PSD. Furthermore, it is noted that the PSD obtained using the FWT model is mainly dependent on the strength of the adsorption potential, while the PSD obtained using the spherical probe method is independent of this quantity. Accordingly, the larger pore size determined by the former technique compared with the geometrical PSD is due to the highly disordered nature of the reconstructed microstructure that leads to lower carbon atomic density and, therefore, to cause weaker adsorption potential strength than that of a graphitic surface. This can be seen for the systems C and D in the work of Figueroa-Gerstenmaier [35]. Meanwhile, in spite of the similar right shift of the predicted PSD using the IWT model in comparison with the geometrical PSD, the predicted PSD derived from the IWT model underestimates significantly the intensity of the geometrical PSD.

5. Molecular dynamics simulations

In this section, we present the results of self-diffusivity of argon at 87 K and nitrogen at 77 K in the reconstructed carbon (CS1000a) using EMD simulation. In the simulation, we utilized fluid–fluid and solid–fluid LJ interaction parameters for argon and nitrogen similar to those used by Pikunic *et al.* [17]. These LJ parameters are listed in Table 1. The cut off radius for fluid–fluid and solid–fluid interactions is 12.4 Å. The canonical ensemble, whereby number of particles, volume of the system and temperature are kept constant, is employed. The system temperature is controlled using a Gaussian

Downloaded At: 18:02 14 January 2011

Downloaded At: 18:02 14 January 2011

Table I. Lennard–Jones parameters for argon and nitrogen used in the EMD simulations in the current work.

Interaction	σ_f (Å)	ε_f/k (K)	*Interaction*	σ_{cf} (Å)	ε_{cf}/k (K)
Ar–Ar	3.41	120	Ar–C	3.38	58
N_2–N_2	3.75	95.20	N_2–C	3.36	61.4

thermostat [36]. The equations of motion are solved using a 5th order Gear predictor–corrector integrator with a time step of 4.5 fs. The results of self-diffusivity are obtained by averaging intermediate results from 1×10^7 time steps. Each result of self-diffusivity is then obtained by averaging repeated runs with distinct initial configurations.

Initial configurations used for EMD simulations were generated by GCMC simulations. Unlike a simple slit pore, for the disordered structure of the reconstructed carbon (CS1000a) insertion trial steps in conventional GCMC simulation might insert particles into closed pores or cavities. This leads to an underestimation of self-diffusivity at low loading. In order to investigate impact of the closed pores on self-diffusivity we may perform particle insertions at an arbitrarily chosen subset of the total simulation volume. In the current work, the subset is selected to be a small region near the boundaries of the simulation volume. Periodic boundary convention (PBC) was applied. In this method, initial configurations for EMD simulation are generated. In this case, the EMD simulations are run for $1.5–2 \times 10^7$ steps in which $0.5–1 \times 10^7$ steps are run for equilibration.

In the current work, all the EMD simulations are run with different loadings ranging from 25 to 90%. Here the loading is defined as ratio of adsorbed quantity, Γ, to that at maximum coverage, Γ_0, defined as the adsorbed amount at 1 atm. For argon at 87 K and nitrogen at 77 K Γ_0 has the value of 12.255 and 10.122 nm^{-3}, respectively.

Figure 11 depicts the results of self-diffusivity of argon at 87 K and nitrogen at 77 K in the reconstructed carbon against loading. The latter is obtained using the initial configurations prepared from the conventional and modified GCMC simulation. From this figure, it can be seen that there exists a maximum in the value of self-diffusivity at 65% loading for argon and nitrogen. The maximum in self-diffusivity observed for nitrogen and argon arises from high heterogeneity of the reconstructed carbon, which may lead to local strong adsorption sites such as small cavities whose size is slightly larger than the adsorbate molecule size. When the fluid particles are exposed to the solid phase, they are rapidly adsorbed in these sites, leading to significant reduction in their mobility. Further increase in loading leads to increase in mobility of the adsorbate molecule due to decrease in the number of strong adsorption sites. Accordingly, self-diffusivity increases with loading in the interval ($<65\%$). This is supported by the fact that a steady decrease in the isosteric heat of adsorption occurs in this region, as seen in figure 12. The isosteric heat, q_{st}, was calculated from the well-known fluctuation formula [37], expressed as:

$$q_{st} = RT - \frac{\langle U_{sf}N\rangle - \langle U_{sf}\rangle\langle N\rangle}{\langle N^2\rangle - \langle N\rangle^2} - \frac{\langle U_{ff}N\rangle - \langle U_{ff}\rangle\langle N\rangle}{\langle N^2\rangle - \langle N\rangle^2}$$

where the quantities in angle brackets are ensemble averages. U_{sf} and U_{ff} are solid–fluid and fluid–fluid interaction energy, respectively. N is number of adsorbate molecules. The term RT represents the ideal gas part arising from translational motion of adsorbate molecules.

At high loading (85%) the number of strong adsorption sites is minimized and collision between adsorbate molecules is predominant. This leads to a decrease in self-diffusivity, as large frequency of inter-atomic collisions leads to rapid decrease in self-correlation of the particle velocity. In addition, the curve of isosteric heat of adsorption in figure 12 shows an increase in the value of isosteric heat of adsorption at high loading. Such an increase in isosteric heat of adsorption was experimentally observed for argon adsorption in MCM 41 at similar condition [38]. Accordingly, the above observation is due

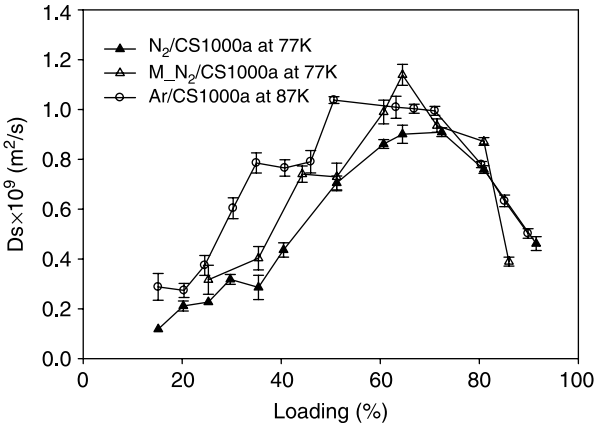

Figure 11. Self-diffusivity of argon at 87 K (open circles) and nitrogen at 77 K (triangles) in the reconstructed carbon (CS1000a) with increasing loading. Filled triangles depict self-diffusivity obtained using initial configuration generated by conventional GCMC simulation, and open triangles that obtained using initial configuration generated by local insertion at the box surface used in the GCMC simulation.

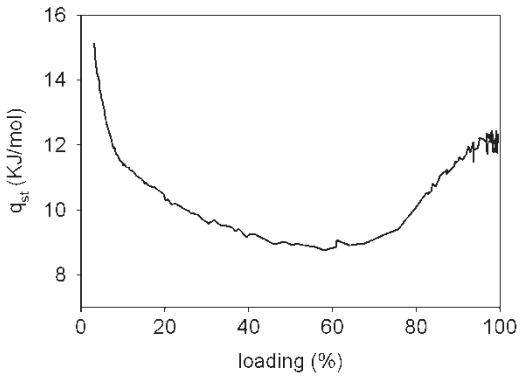

Figure 12. Isosteric heat of argon adsorption at 87 K in the reconstructed carbon, obtained using the large simulated system (566 carbon atoms), with loading.

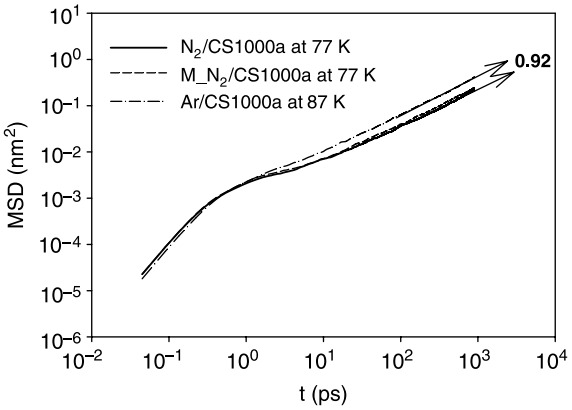

Figure 13. Mean square displacement (MSD) versus time (t): N_2 (solid line) adsorbed in the reconstructed carbon (CS1000a) at 77 K using initial configuration generated by conventional GCMC simulation, (dashed line) using local insertion at the box surface in the GCMC simulation, and Ar (dashed-dotted line) adsorbed in the carbon at 87 K.

to the occurrence of condensation in the larger pores (>9 Å), as seen in figure 10b.

As seen in figure 11, the self-diffusivity of nitrogen, obtained with initial configuration prepared using modified GCMC simulation, is slightly higher than that using conventional GCMC simulation at low loading (<80%) and lower at high loading (85%). This suggests that there exists a small portion of closed porosity in the carbon, that gives rise to slightly higher number of adsorbate molecules in the open or connected pore space, with the initial configuration prepared using the modified GCMC simulation, compared with that using conventional GCMC simulation. A higher number of particles in the connected pore space in the former case leads to faster diffusion at low loading and slower diffusion at higher loading (where strong fluid–fluid interactions reduce mobility). Finally, it is interesting to observe that self-diffusivity of nitrogen obtained in the current work is almost an order of magnitude larger than that reported by Pikunic *et al.* [5] for CS1000 at the same condition. The CS1000 was a semi-coke sample, obtained by pyrolysis of pure saccharose at 1000°C under nitrogen flow. The higher diffusivities found here are consistent with the larger average pore size of CS1000a compared with that of the unactivated carbon used by these authors [15]. Further, the higher diffusivity of nitrogen in the current work can be also due to the higher degree of graphitization as well as higher porosity of the activated form investigated (0.583 compared with 0.088, as reported by Pikunic *et al.* [15]). The results of self-diffusivity of argon in the current work are about 3–4 times smaller than that in slit pores with atomistic walls, reported by Krishnan and Ayappa [39] for similar pore size. Slower diffusion is expected due to the pore topology and tortuosity of the carbon model, which is not considered in the slit–pore model. Further, reflection coefficients are expected to be considerably larger for the highly disordered carbon investigated here, in comparison to that for the relatively smooth graphitic surfaces of slit pores.

A feature of the self-diffusion coefficients to be noted here is that they are Fickian, as was evidenced by the slope of the plot of mean squared displacement versus time, as illustrated in figure 13. The long time limit of this slope was approximately 0.92 over the loading range investigated, which agrees with the expected slope of unity for Fickian diffusion.

6. Conclusions

We have illustrated reconstruction of a low-density saccharose-based activated carbon (CS1000a) using the HRMC method for small and large systems that comprise 125 and 566 carbon atoms respectively. From results gained from the small system, we proposed a two-step reconstruction procedure. In the first step, the HRMC algorithm with energetically favored weight is applied to generate an initial configuration that has minimized the fraction of three-member rings while its pair correlation function matches reasonably the corresponding experimental one in the long-range region. This initial configuration is then used with the HRMC algorithm at constant temperature ($T = 300$ K) and weighting parameter ($\sigma = 0.05$). Although an excellent fit between the pair correlation function and the corresponding experimental one is obtained using in our current work, further investigation on dependence of the converged configuration on initial configuration is necessary.

An independent validation of the accuracy of the FWT and IWT models for determination of PSD of the reconstructed carbon model was conducted in this work. The results showed superiority of the FWT model to IWT model in terms of providing PSD result closer to the geometric one, although shift of the FWT derived PSD to larger pore size compared with the (exact) geometric PSD is observed, due to the highly disordered nature of the reconstructed carbon. Self-diffusivity of argon at 87 K and nitrogen at 77 K in the reconstructed carbon using EMD simulation was found to be about one order of magnitude faster than that reported by Pikunic *et al.* [5] for the low porosity carbon CS1000, but is about 3–4 times lower than that in slit-pores of similar size due to the effects of pore topology and tortuosity.

Acknowledgements

This research has been supported by grants from the Australian Research Council under the Discovery Scheme (grant no. DP0556342), and from the US National Science Foundation (grant no. CTS-0211792). Thanh Nguyen acknowledges a Travel Scholarship from the University of Queensland, which enabled this collaboration.

References

[1] G. Opletal, T. Petersen, B. O'Malley, I. Snook, D.G. McCulloch, N.A. Marks, I. Yarovsky. Hybrid approach for generating realistic

Downloaded At: 18:02 14 January 2011

amorphous carbon structure using Metropolis and reverse Monte Carlo. *Mol. Simul.*, **28**, 927 (2002).
[2] N.A. Marks. Generalizing the environment-dependent interaction potential for carbon. *Phys. Rev. B*, **63**, 035401 (2000).
[3] N.A. Marks. Modelling diamond-like carbon with the environment-dependent interaction potential. *J. Phys.: Condens. Matter*, **14**, 2901 (2002).
[4] T.X. Nguyen, S.K. Bhatia. Probing the pore wall structure of nanoporous carbons using adsorption. *Langmuir*, **20**, 3532 (2004).
[5] J. Pikunic, K.E. Gubbins. Molecular dynamics simulations of simple fluids confined in realistic models of nanoporous carbons. *Eur. Phys. J. E*, **12**, 35 (2003).
[6] T.X. Nguyen, S.K. Bhatia. Characterization of activated carbon fibers using argon adsorption. *Carbon*, **43**, 775 (2005).
[7] J.P. Olivier. Modeling physical adsorption on porous and nonporous solids using density functional theory. *J. Porous Mater.*, **2**, 9 (1995).
[8] P.I. Ravikovitch, J. Jagiello, D. Tolles, A.V. Neimark. DFT methods for micropore size characterization of activated carbons: role of pore wall heterogeneity. *Carbon'01, International Conference on Carbon*, Lexington (2001).
[9] T.X. Nguyen, S.K. Bhatia. Characterization of pore wall heterogeneity in nanoporous carbons using adsorption: the slit–pore model revisited. *J. Phys. Chem. B*, **108**, 14032 (2004).
[10] T.X. Nguyen, S.K. Bhatia. Characterization of heat-treated porous carbons using argon adsorption. *Carbon*, **44**, 646 (2005).
[11] T.X. Nguyen, S.K. Bhatia, D. Nicholson. Prediction of high-pressure adsorption equilibrium of supercritical gases using density functional theory. *Langmuir*, **21**, 3187 (2005).
[12] K. Malek, M.-O. Coppens. Effects of surface roughness on self- and transport diffusion in porous media in the Knudsen regime. *Phys. Rev. Lett.*, **87**, 125505 (2001).
[13] R.L. McGreevy, L. Putsai. Reverse Monte Carlo simulation: a new technique for the determination of disordered structures. *Mol. Simul.*, **1**, 359 (1988).
[14] K.T. Thomson, K.E. Gubbins. Modelling structural morphology of microporous carbons by reverse Monte Carlo. *Langmuir*, **16**, 5761 (2000).
[15] J. Pikunic, C. Clinard, N. Cohaut, K.E. Gubbins, J.-M. Guet, R.J.-M. Pellenq, I. Rannou, J.-N. Rouzaud. Structural modeling of porous carbons: constrained reverse Monte Carlo method. *Langmuir*, **19**, 8565 (2003).
[16] J. Pikunic, K.E. Gubbins, R.J.-M. Pellenq, N. Cohaut, I. Rannou, J.-M. Guet, C. Clinard, J.-N. Rouzaud. Realistic molecular models for saccharose-based carbons. *Appl. Surf. Sci.*, **196**, 98 (2002).
[17] J. Pikunic, P. Llewellyn, R.J.-M. Pellenq, K.E. Gubbins. Argon and nitrogen adsorption in disordered nanoporous carbons: simulation and experiment. *Langmuir*, **21**, 4431 (2005).
[18] S.K. Jain, J. Fuhr, R.J.-M. Pellenq, J. Pikunic, C. Bichara, K.E. Gubbins. Stability study of porous carbon structures obtained from reverse Monte Carlo using tight binding and bond order Hamiltonians. *Stud. Surf. Sci. Catal.* (2006) (in press).
[19] S.K. Jain, J. Pikunic, R.J.-M. Pellenq, K.E. Gubbins. Effects of activation on the structure and adsorption properties of a nanoporous carbon using molecular simulation. *Adsorption*, **11**, 355 (2005).
[20] G. Opletal, T.C. Petersen, D.G. McCulloch, I.K. Snook, I. Yarovsky. The structure of disordered carbon solids studied using a hybrid reverse Monte Carlo algorithm. *J. Phys.: Condens. Matter*, **17**, 2605 (2005).
[21] T.C. Petersen, I. Yarovsky, I. Snook, D.G. McCulloch, G. Opletal. Structural analysis of carbonaceous solids using an adapted reverse Monte Carlo algorithm. *Carbon*, **41**, 2403 (2003).
[22] T. Petersen, I. Yarovsky, I. Snook, D.G. McCulloch, G. Opletal. Microstructure of an industrial char by diffraction techniques and reverse Monte Carlo modeling. *Carbon*, **42**, 2457 (2004).
[23] S.K. Jain, K.E. Gubbins, R.J.-M. Pellenq, J.P. Pikunic. Molecular modeling of porous carbons using hybrid reverse Monte Carlo. *Langmuir*, (in press).
[24] D.W. Brenner. Empirical potential for hydrocarbons for use in simulating the chemical vapor deposition of diamond films. *Phys. Rev. B.*, **42**, 9458 (1990).
[25] A.K. Soper. An amateur guide to the pitfalls of maximum entropy. *Inst. Phys. Conf. Ser.*, **107**, 57 (1990).
[26] S. Kilpatrick. Optimization by simulated annealing. *Science*, **220**, 671 (1983).
[27] N.A. Marks, D.R. McKenzie, B.A. Pailthorpe. Microscopic structure of tetrahedral amorphous carbon. *Phys. Rev. Lett.*, **76**, 768 (1996).
[28] D.S. Franzblau. Computation of ring statistics for network models of solids. *Phys. Rev. B*, **44**, 4925 (1991).
[29] S.J. Stuart, A.B. Tutein, J.A. Harrison. A reactive potential for hydrocarbon with intermolecular interactions. *J. Chem. Phys.*, **112**, 6472 (2000).
[30] N.A. Marks, N.C. Cooper, D.R. McKenzie. Comparison of density-functional, tight-binding and empirical methods for the simulation of amorphous carbon. *Phys. Rev. B*, **65**, 075411 (2002).
[31] M.T. Knippenberg, O. Kum, S.J. Stuart. Structural study of amorphous carbon using adaptive interatomic reactive empirical bond-order potential model. *NSTI Nanotechnology Conference and Trade Show*, Anaheim (2005).
[32] J.H. Los, A. Fasolino. Intrinsic long-range bond-order potential for carbon: Performance in Monte Carlo simulations of graphitization. *Phys. Rev. B*, **68**, 024107 (2003).
[33] L.D. Gelb, K.E. Gubbins. Pore size distribution in porous glasses: a computer simulation study. *Langmuir*, **15**, 305 (1999).
[34] R.J. Dombrowski, D.R. Hyduke, C.M. Lastoskie. Pore size analysis of activated carbons from argon and nitrogen porosimetry using density functional theory. *Langmuir*, **16**, 5041 (2000).
[35] S. Figueroa-Gerstenmaier, J.B. Avalos, L.D. Gelb, K.E. Gubbins, L.F. Vega. Pore size distribution of porous glasses: a test of the independent pore model. *Langmuir*, **19**, 8592 (2003).
[36] D.J. Evans, G.P. Morriss. *Statistical Mechanics of Nonequilibrium Liquids*, Academic, London (1990).
[37] D. Nicholson, N.G. Parsonage. *Computer simulation and the statistical mechanics of adsorption*, p. 97, Academic Press, London (1982).
[38] J.P. Olivier. Comparison of the experimental isosteric heat of adsorption of argon on mesoporous silica with density functional theory calculations. *Stud. Surf. Sci. Catal.*, **128**, 81 (2000).
[39] S.H. Krishnan, K.G. Ayappa. Modeling velocity autocorrelation functions of confined fluids: a memory function approach. *J. Chem. Phys.*, **118**, 690 (2003).

Downloaded At: 18:02 14 January 2011